THE JOURNAL OF PHYSICAL CHEMISTRY C
A JOURNAL OF THE AMERICAN CHEMICAL SOCIETY

pubs.acs.org/JPCC

Article

Atomic-Scale Finite-Element Modeling of Elastic Mechanical Anisotropy in Finite-Sized Strained Phosphorene Nanoribbons

Krzysztof Pyrchla* and Robert Bogdanowicz

Cite This: J. Phys. Chem. C 2022, 126, 14219−14228

Read Online

ACCESS | Metrics & More | Article Recommendations

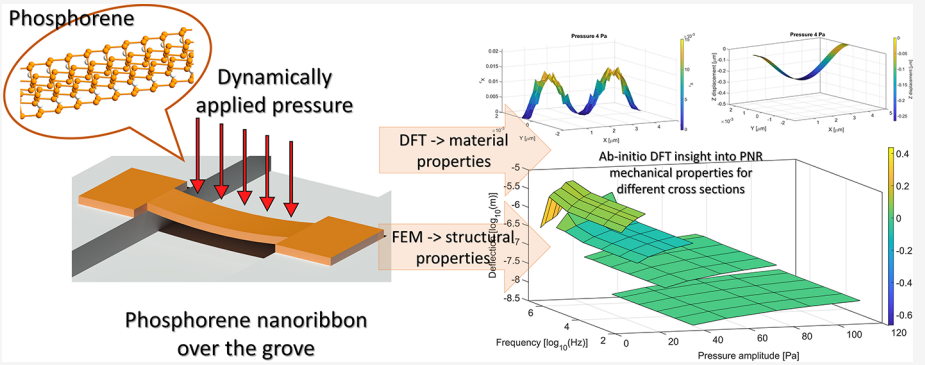

ABSTRACT: Nanoribbons are crucial nanostructures due to their superior mechanical and electrical properties. This paper is devoted to hybrid studies of the elastic mechanical anisotropy of phosphorene nanoribbons whose edges connect the terminals of devices such as bridges. Fundamental mechanical properties, including Young's modulus, Poisson's ratio, and density, were estimated from first-principles calculations for 1-layer, 3-layer, and 6-layer nanoribbons with widths of 10 Å. The data achieved from the ab initio simulations supplied the finite-element model (FEM) of the nanoribbons. The directional coefficients of strain pressure curves were estimated as Young's effective modulus since the structure is one-dimensional (1D). The modulus values were equal to 85.8, 111.8, and 134 GPa for 6, 3 and 1 layers, respectively. Moreover, the variation in Poisson's coefficient for the armchair direction was significantly smaller than for the zigzag direction. Monotonic changes in this twist were observed for structures with 3 and 6 layers within the plane along the zigzag axis. The phosphorene nanoribbons subjected to periodic excitation behaved similarly to those subjected to static loading, while their whippiness was inversely proportional to the length. Next, the deflection under static force, resonance frequencies, and response to a variable driving force were calculated.

1. INTRODUCTION

Phosphorene is a novel two-dimensional (2D) material that was given its name by analogy with graphene. This material demonstrates sp^3 hybridization, in contrast to sp^2 graphene, but shares its superior electrical properties. Since its first fabrication, numerous different possible applications have been found in electronics,[1] optics, and biotechnology. It has been shown that this material has excellent mechanical properties, can be stretched up to 30% before breaking, and can withstand significant pressures. All of these similarities to graphene suggest that phosphorene should be an outstanding material for nanoribbon production.

Phosphorene nanoribbons (PNRs) are one-dimensional (1D) materials that are scientifically attractive due to their properties that are a compromise between high career mobility and a semiconductor, which enables them to be used to build phosphorene field-effect transistors (FETs) with a high on/off ratio. Various techniques of phosphorene nanoribbon production are continuously under development. The fabrication of phosphorene nanoribbons was recently reported using various approaches, such as ionic scissoring, one-step chemical vapor transport (CVT) synthesis, electron beam sculpture, and electrochemical exfoliation.[2−5] Each method leads to the production of nanoribbons with slightly different properties. The crucial factor is the dimensions of the nanoribbons that can be produced via each method. Furthermore, CVT synthesis, ionic scissoring, and electrochemical exfoliation lead to the creation of a population of nanoribbons with some variation in properties. The applicability of PNRs is an issue.

Received: June 28, 2022
Revised: July 28, 2022
Published: August 12, 2022

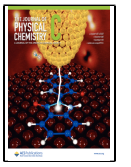

The key factor is the geometrical dimensions of the nanoribbons that can be obtained through each method. For example, the electron beam sculpting method results in 15 nm long ribbons, but their spatial separation is weak. Electron beam lithography techniques produce ribbons with widths of 60 nm and heights of 3 nm, so they behave like bulk black phosphorus rather than few-layer phosphorene. Significantly better results can be achieved by the application of liquid exfoliation (the "ionic scissoring" approach),[2] especially when followed by intercalation of the phosphorus layer with alkali metals such as Li. This method leads to the fabrication of a broad spectrum of nanoribbons with lengths up to 11 μm and aspect ratios up to 1000. Nevertheless, this material is a challenge to scale the fabrication process.

Shaping 2D materials at the nanoscale unlocks new properties and effects. In the phosphorene structure, after its limitation to one dimension in a zigzag direction (ZDPNR), new electron tunneling paths unlock. As a result, the spin-dependent Seebeck effect arises.[6] Multiple essential parameters, both mechanical and electrical, can be changed by adjusting the geometrical dimensions of the structure. The band gap of the structure is directly connected with the nanoribbon width, and the scaling law is different for both possible orientations of the ribbon.[7]

Because of their unique properties, PNRs have been continuously under both theoretical and experimental investigation. The majority of the experiments have been focused on phosphorene structural anisotropy, which is reflected in many of its properties. The anisotropy of the thermal conductance is one well-documented example,[8] followed by the anisotropy of mechanical parameters such as Young's modulus and Poisson's ratio.[9] The anisotropy of thermal conductance can be explained as a result of strong anisotropy in Young's modulus of phosphorene since the thermal conductance is determined in this material by the phonon group velocity, which is related to Young's modulus.[10]

Research into the optical properties of PNRs has also revealed many interesting properties, such as the formation of exciton funnels after the application of a specific strain force to the nanoribbons.[11] It has also been reported that many important properties of phosphorene, such as its optical absorption,[12] Raman spectrum,[13,14] electrical conductance,[15] and electron band structure, are sensitive to tensile strain.

Since the properties of phosphorene are dependent on the strain, the 1D configuration is desired because it allows the applied strain direction to be controlled. Using the currently known experimental techniques, it is possible to form nanoribbons in a "bridge" arrangement over a groove on a silicon substrate.[16] A complete review,[9] presenting the problem of mechanical properties, was mainly focused on the properties of such PNRs, whose dimensions can be measured in microns. This approach is reasonable since nearly all PNRs fabricated thus far are technically nanobelts.[17] Moreover, since the multiple electrooptical properties of PNRs are size-dependent,[18] current progress in the production of PNRs is focused on achieving structures with higher aspect ratios.[2]

Many simulations have been performed to estimate basic mechanical properties, such as Young's modulus.[9,19−21] However, most of this work has been focused on nanolayers (2D crystal structure) and bulk structures. There is a significant lack of work done with regard to estimations of the properties of few-layer black PNRs, especially those that shrink by a few nanometers in width. There have been attempts to experimentally measure Young's modulus of free-standing nanoribbons,[9,16] but the structures being examined have cross-sectional dimensions of tens of nanometers (nm) × tens of nanometers. Taking this into account, density functional theory (DFT) simulations can be considered a reliable source of information about the mechanical properties of few-layer PNRs, with a few-nanometer width.

There is a significant difference in mechanical behavior between micro- and nanostructures.[22] This is caused by edge-related effects, which are significant only for narrow nanoribbons.[23] The edge stress accumulation can be an example of such an effect. For both a bulk structure and 2D nanolayers, theoretical work employing the ab initio DFT method for the calculation of Young's modulus and Poisson's ratio is in good agreement with the experimental data.[24] Thus, it can be assumed that DFT-calculated mechanical properties for PNR structures should also be close to actual values. Taking this into account, a decision was made to directly model both the Young's modulus and Poisson's ratio of 1 nm nanoribbons and not extrapolate experimental data gathered for larger structures.

The most reliable way to analyze the mechanical behavior of the nanostructures is through experiments and then molecular dynamics simulations. Notably, simulations of the dynamical behavior of complex nanomechanical systems are computationally demanding, and controlled experiments conducted at the nanoscale are extremely difficult. Since each nano-opto-electro-mechanical system (NOEMS) design has to be proven to work before it was even constructed, to avoid unreasonable losses, simulations in conium approximation were proposed as a solution.[25−32]

In this work, a synergistic (DFT + FEM) study of the elastic and mechanical anisotropy of suspended PNRs was presented. The designed elastic PNR resonator is connected to both terminals in the form of a bridge. The mechanical properties of ultrathin phosphorene ribbons are dependent on the ribbon cross section. Thus, basic mechanical properties, such as Young's modulus, Poisson's ratio, and density, are first estimated from first-principles calculations for 1-layer, 3-layer, and 6-layer 10 A wide nanoribbons utilizing the DFT method. The data achieved from the ab initio DFT simulations were utilized as an input for the finite-element model (FEM) of the nanoribbons. The static deflection under homogeneous pressure, normal modes, and response to dynamic force are presented. The results achieved during simulations allow us to determine the vibrational behavior of the PNR by revealing how much space each vibration mode requires for its existence. This provides information regarding the minimum requirements for the size of the groove below the PNR.

This ab initio approach for mechanical property estimation has already proven effective in cases when no experimental data are available. On the other hand, FEM vibrational analysis is also a mature numerical technique proven to be efficient in solving large-scale problems. The main idea of this article is to combine the benefits of both methods to describe the mechanical behavior of narrow PNRs efficiently.

2. METHODS

2.1. DFT Structure Modeling. The structure was modeled using two separate approaches. First, an atomic-scale model was prepared for the purpose of ab initio simulation. This part of the simulation was conducted to evaluate the mechanical properties (Young's modulus, Poisson's modulus, and density)

https://doi.org/10.1021/acs.jpcc.2c04500
J. Phys. Chem. C 2022, 126, 14219−14228

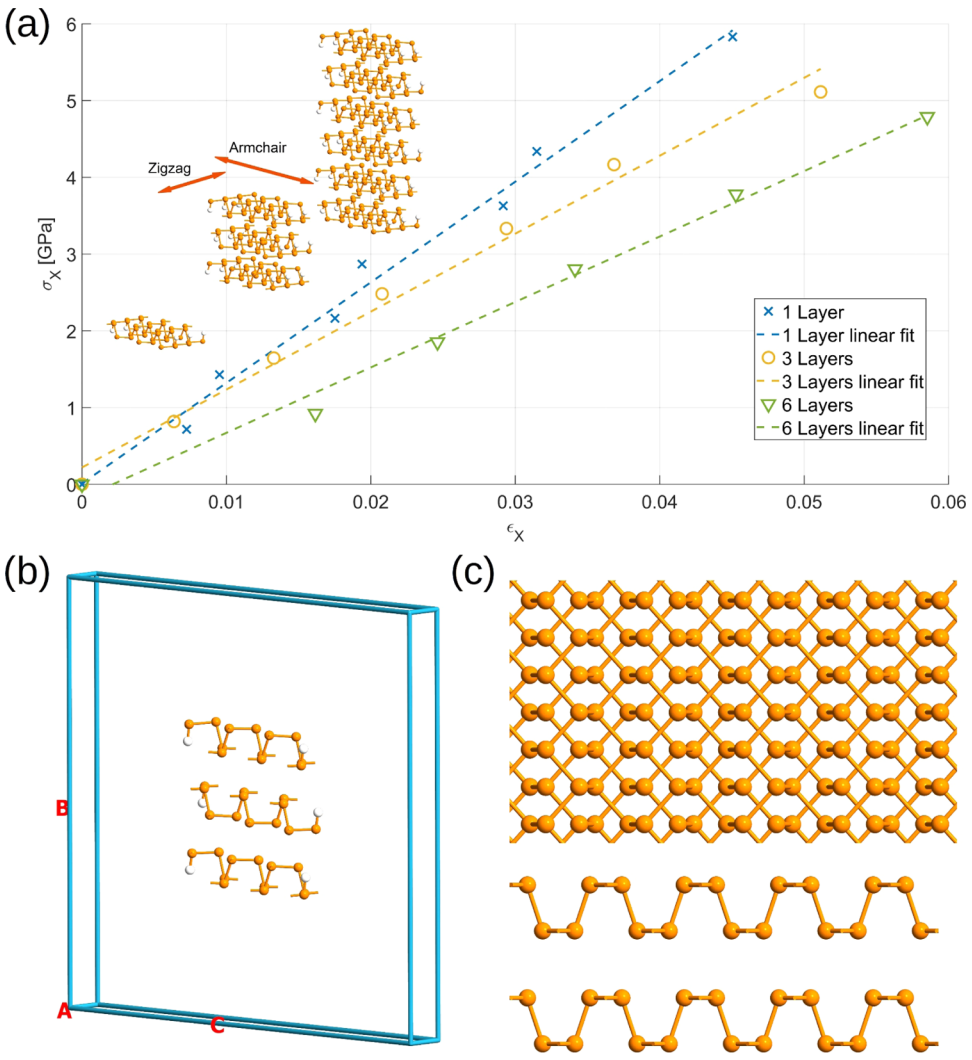

Figure 1. DFT examination of mechanical properties: (a) stress−strain curve for phosphorene 1, 3, and 6 layers, 10 Å width zigzag nanoribbon; (b) unit cell of the 3-layer nanoribbon used during computations; and (c) T_b stacking principle of phosphorene.

of the ultrathin nanoribbon, which were then used during FEM simulation of the nanoribbon.

During the experiment, the interatomic forces were calculated using the ab initio approach within DFT with a linear combination of atomic orbitals (DFT-LCAO). For the purpose of the DFT calculation, Perdew−Burke−Ernzerhof (PBE) functionals were used. Because the model was 1D infinite, the *k*-point sampling was anisotropic 4 × 1 × 1 (Monkhorst−Pack). The mesh cut-off energy was set to 160 Ha. All numerical parameters were tested for convergence of the values of the forces before calculation began.

Atomic models were created using the black phosphorus bulk structure from a database. The atomic model structure was prepared by assembling single black phosphorus layers using the T_b stacking principle, which was reported to be most energetically favorable.[33] The stacking order is shown in Figure 1c. The number of layers in the structure was 1, 3, and 6. A single-unit cell represents a phosphorene nanoribbon with a width of 13 Å, and the edges of the ribbon were fully hydrogen-terminated. To simulate a very long nanoribbon, periodic boundary conditions were applied to the cell borders. The length of the ribbon that lies inside the cell was set to 10 Å. The perpendicular direction of the cell was set accordingly to generate an ∼20 Å vacuum buffer around the ribbon.

The resulting structure was optimized using the limited-memory Broyden−Fletcher−Goldfarb−Shanno (LBFGS) algorithm with the condition of zero external pressure. Both the positions of all atoms and the length of the cell in the direction of the ribbon were optimized. The two directions perpendicular to the ribbon were kept fixed during the optimization. Nevertheless, the material was able to both shrink and expand freely in the perpendicular direction due to the vacuum buffer around it. The stop criteria were set both for the values of the forces and the pressure tolerance. The maximum force had to fall below 10^{-4} eV/Å, and the maximum pressure threshold was 10^{-5} eV/Å^3. Both criteria had to be met to stop the LBFGS iterations.

After the structure was relaxed under the zero-pressure condition, the main part of the experiment began. The pressure on the structure was repeatedly increased in equal increments from 1.63 GPa for the 6-layer to 2.35 GPa for the monolayer structure. The exact value of this increment was selected by testing different values and checking the coverage of the results. To achieve more data points for $\varepsilon < 0.05$, further refinement was conducted. Additional optimizations were

https://doi.org/10.1021/acs.jpcc.2c04500
J. Phys. Chem. C 2022, 126, 14219−14228

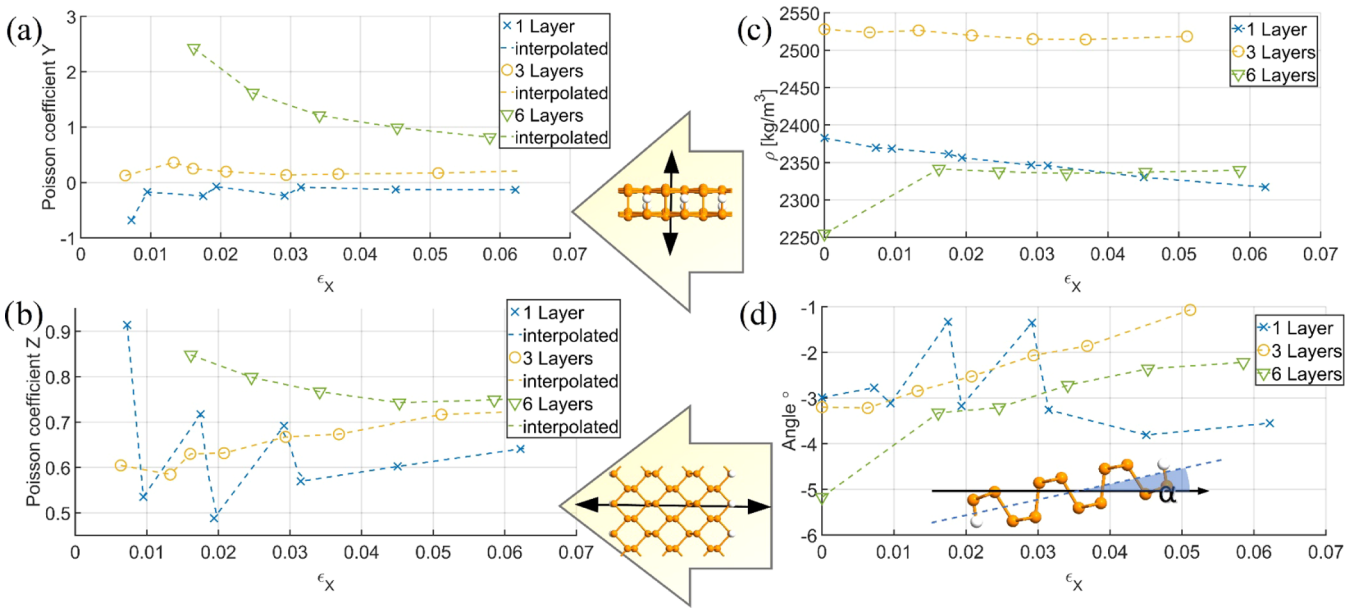

Figure 2. Basic mechanical properties of the PNR: (a) Poisson's ratio on the *Y* axes; (b) Poisson's ratio on the *Z* axes. Direction *Y* is perpendicular to the plane, *X* is zigzag, and *Z* is armchair; (c) changes in the mean density of the nanoribbon under strain; and (d) twist angle of the PNR during straining. The insets present how this angle is defined.

applied for the pressure selected based on the current $\sigma(\varepsilon)$ curve. This approach is important for two reasons: (1) it generates new data points in the zone of linear material response and (2) new points lie on the same curve as previously generated, proving the convergence of this approach.

For each step, the geometry optimization was repeated using the structure from the previous step as a starting guess. If the pressure was too high and the optimization ripped the structure apart, then there was an additional stop criterion (in addition to the obvious criterion of the maximal iteration for each LBFGS) that stopped the calculation if the relative deflection exceeded an a priori set threshold. In such cases, the structure was optimized once again but with an increment in the pressure cut in half.

The described procedure was repeated for structures with different numbers of layers, and the strain−stress curves were obtained for each structure (Figure 1). By analyzing the geometric dimensions of the structure, more important mechanical properties can be found, such as Poisson's ratio and the density. Moreover, the structure's twist along its length can also be predicted.

2.2. Microstructural FEM Modeling. The deviation of the material's properties from the atomic-scale simulation was used for the microscale simulation of a phosphorene ribbon. The geometry of the structure was prepared as a thin prism with 1 nm width, 5 μm length, and 1.65 nm thickness. The deflection under the static force, resonance frequencies, and response to a variable driving force were calculated using the FEM. During this step, the MATLAB PDE toolbox was utilized as the computation engine.

The simulation applying FEM was a static response analysis. The structure was slightly extended by the addition of small anchoring sheets of material at the ends. These anchors were 0.5 μm wide and 0.05 μm long. Some part of the material was adhered to the substrate, but there was a small gap in the substrate, so a small part of the material formed a "membrane" or "bridge"-like structure above it. The behavior of the bridge was simulated, but a smooth transition is needed from a flexible bridge to a rigid part of the material, which was adhered to the substrate. Therefore, the free-standing part of the material above the groove in the substrate was particularly considered.

Then, the side faces of the anchor were fixed, and a constant, homogeneous pressure was applied to the top surface of the material. The resulting node displacement map (Figure 3) was prepared for different ribbon lengths and different pressure magnitudes. During this step, the maximal length of the mesh cell was 10 nm. The deflection map was recalculated to the local strain map (along the direction of the ribbon). One such map is presented in Figure 4.

The next step of the simulation was to find the structure eigenmodes. A solid modal simulation was performed for each ribbon length. To provide a sufficient convergence level, the tightest mesh was used with a 1 nm maximal cell size.

In the last series of simulations, harmonic oscillation pressure acting on the device surface was utilized. This allows the response of the device to an external driving force to be studied. A wide range of frequencies was used, both lower and higher than the resonance frequency.

3. RESULTS AND DISCUSSION

3.1. Material Properties of Few-Layer PNR with a High Aspect Ratio. To understand the influence of pressure on the structure of PNRs, a pressure−strain diagram was made in the zigzag direction, as shown in Figure 1. The diagram was made for three different number of layers in the structure. As expected, there is a relation between the number of layers and the susceptibility to strain in the structure.[19,34] The susceptibility of the material to the applied pressure increases with an increase in the number of layers. This means that for the same pressure values for a material with a higher number of layers, the deformation will be significantly larger. Since the studied structure can be treated as one-dimensional, the directional coefficients of the strain pressure curves can be treated as the Young's effective modulus of the structure. The

https://doi.org/10.1021/acs.jpcc.2c04500
J. Phys. Chem. C 2022, 126, 14219−14228

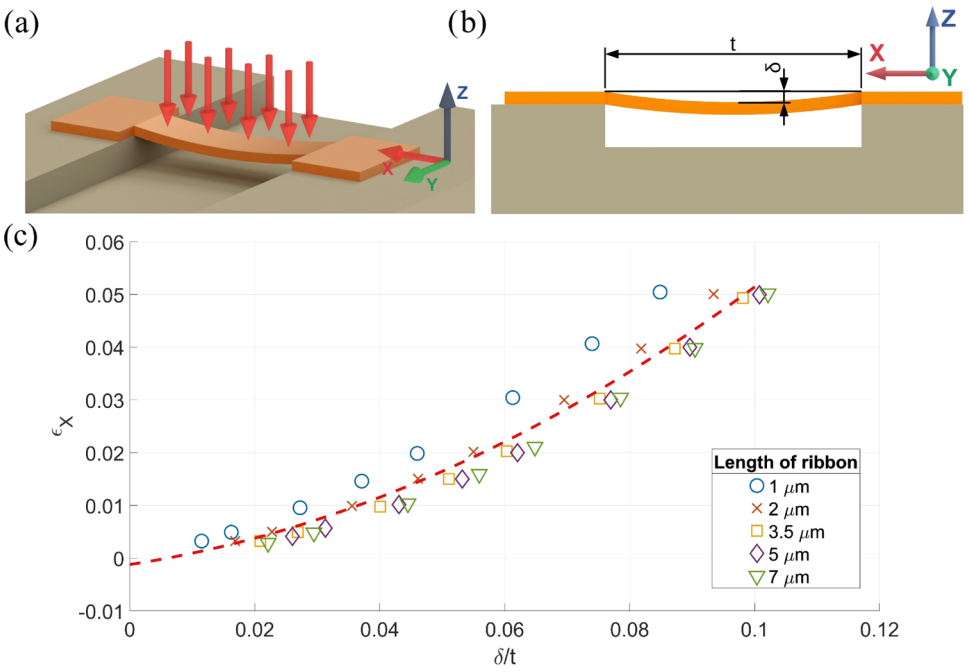

Figure 3. Static pressure response test result: (a) idealized presentation of the case study with the use of the FEM method. The PNR is suspended over the grove; on one of its sides, the static or dynamic distributed load is applied (the load direction is marked by red arrows). (b) Scheme showing how ribbon deflection is defined. (c) Cumulative results showing the relation between the deflection coefficient (deflection divided by ribbon length) and the maximal strain occurring in a ribbon structure.

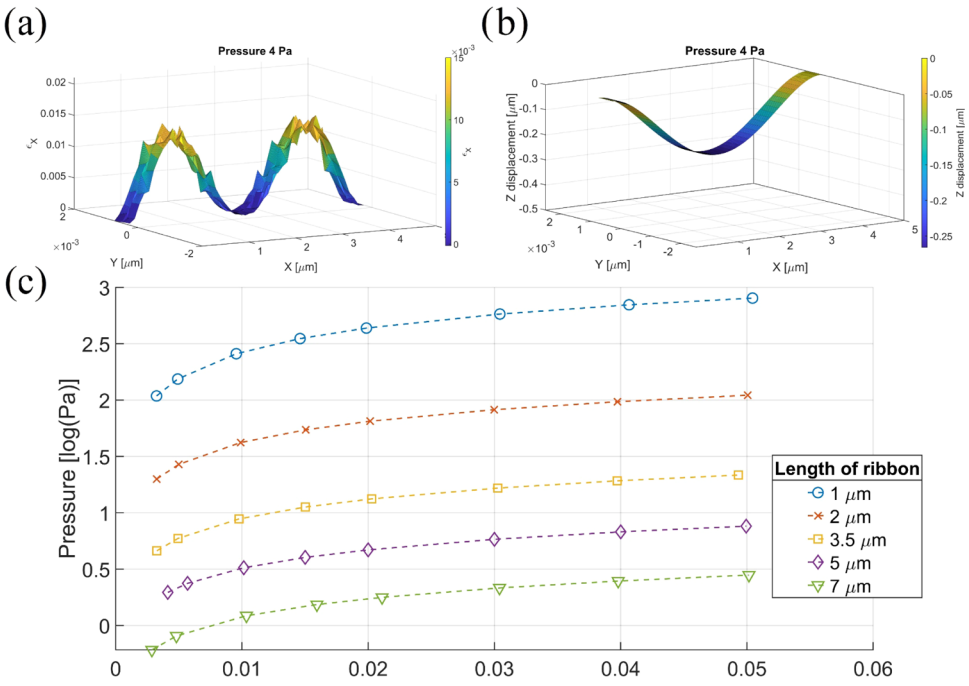

Figure 4. Strain generated by static pressure response test result: (a) distribution of the strain in the PNR under 4 Pa pressure; (b) deflection of the ribbon caused by 4 Pa pressure, and (c) relationship between the strain in the ribbon and pressure applied on its surface.

following Young's modulus values were obtained: 85.8 GPa for 6 layers, 111.8 GPa for 3 layers, and 134 GPa for 1 layer.

Further experimental modeling was conducted to estimate the key mechanical parameters of the PNRs. Changes in the dimensions of the structure in directions perpendicular to the strain were compared with those occurring in the strain direction. This enabled the estimation of Poisson's ratios for the studied nanoribbons. The relationship between the calculated coefficients and strain is shown in Figure 2a,b. A negative Poisson's ratio for the phosphorene monolayer, already reported in the literature,[35,36] was observed in the direction perpendicular to it. The variation in Poisson's coefficient for the armchair direction is significantly smaller, both between structures with different numbers of layers and in relation to the strain. A similar behavior of Poisson's ratio was also observed in the other simulation experiments.[22,37]

https://doi.org/10.1021/acs.jpcc.2c04500
J. Phys. Chem. C 2022, 126, 14219−14228

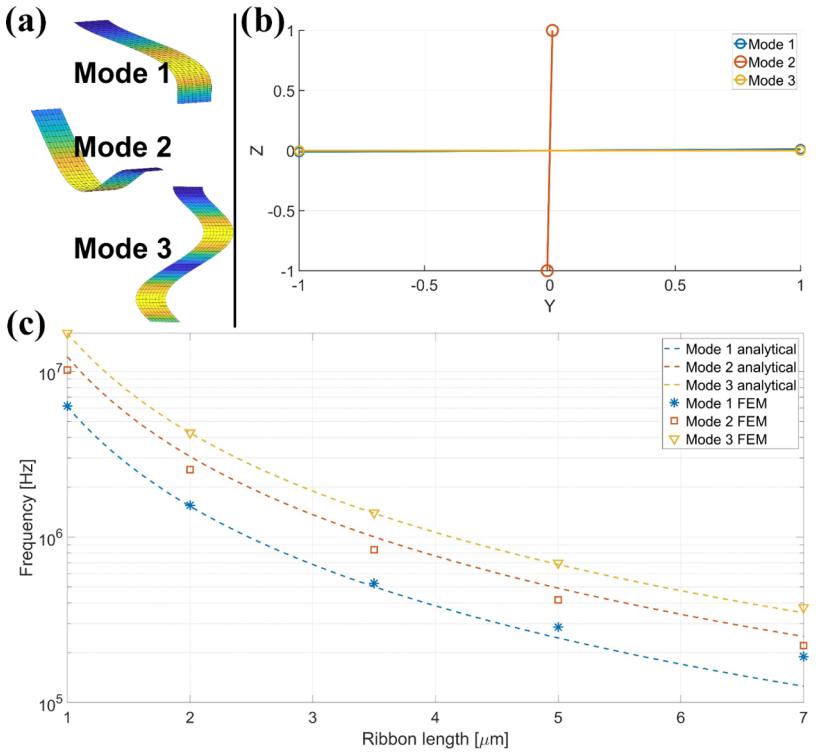

Figure 5. Results of normal mode analysis: (a) three-dimensional (3D) shape of the vibrational modes of the nanoribbon; (b) *YZ* projection for the trajectory of the center of the ribbon during each vibration mode; and (c) normal modes of the phosphorene ribbons calculated analytically and by FEM simulation.

During the data analysis, it was noticed that the structure undergoes a certain twisting dependent on the strain occurring in the structure. Surprisingly, the twisting phenomenon of phosphorene nanoribbons was attributed to their anisotropic properties.[38] This kind of twisting should not be confused with twists used for the generation of Moiré patterns in phosphorene. The twist in our experiments does not occur between planes (as required for Moiré patterns[39]) but within the plane along the zigzag axis. This type of twisting was not observed in linearly strained phosphorene 2D layers[40] but was observed in strained graphene ribbons.[41]

The process of such twisting is attributed to the edge stress.[24] The edge stress is an important factor since it can overcome the plane stiffness and lead to ribbon curling, which was observed in graphene nanoribbons.[23] However, studies conducted thus far suggest that phosphorene plane stiffness is significantly greater than for graphene, which is attributed to the PNR puckered structure. The PNR is most likely to accumulate edge stress rather than release it in the restructuring process.[37] The effect of this accumulation is observed in the twisting of the structure.

Monotonic changes in this twist were observed for structures with 3 and 6 layers. For the single-layer material, no clear tendency appeared. A plot of the dependence of the structure twist on the strain is shown in Figure 2d. The structure density was also calculated (Figure 2c).

3.2. PNR Bridge Static and Dynamic Properties at the Microscale. Based on the DFT-estimated PNR structure parameters, an FEM model of the PNR was created. The FEM method is known for being a successful tool in solving the problems of mechanical property estimation of a macroscopic object. However, there are some reported successful applications of this method for submicron-scale analysis.[42−45] The first experiment carried out using this model was a static test of its loading (Figure 3a). This enabled the determination of the deflection extent of the nanoribbon when subjected to external pressure and the correlation of this deflection to the strain in the nanoribbon. Similar to other works,[16] as a measure of ribbon deflection, the unitless parameter δ/t was introduced. This parameter is the deflection (δ) of the ribbon divided by its length (see Figure 3b). The strain distribution within the PNR was examined during its deflection by tracing the relative change in length of FEM mesh edges. The shape of the strain map is shown in Figure 4a. In Figure 3c, the strain value refers to the maximal strain observed within the ribbon at a particular deflection.

There have been attempts to measure the static mechanical response of few-layer phosphorene by means of mechanical nanoindentation,[34] but there are no existing direct measurements for structures with small widths in comparison to their length (i.e., high aspect ratio).

The mechanical strain is distributed similarly in every case, so the shape presented in Figure 4a is the same for every pressure applied to the ribbon, and only the magnitude of strain changes.

Natural vibration analysis of the nanoribbon structure was carried out. On this basis, the shape and frequency of the first three modes of natural vibrations were calculated. The shape of the modes is shown in Figure 5a, while their frequencies are displayed in Figure 5c. The focus was on the analysis of forces acting perpendicular to the surface on which the nanoribbon is built. This direction of application of an external force is most likely under real conditions since most of the fabricated nanoribbons are grown at the substrate, which is parallel to its layers.[17,18,46] Taking into account the low thickness of the layer and the fact that it is partially adhered to the substrate, we only

https://doi.org/10.1021/acs.jpcc.2c04500
J. Phys. Chem. C 2022, 126, 14219−14228

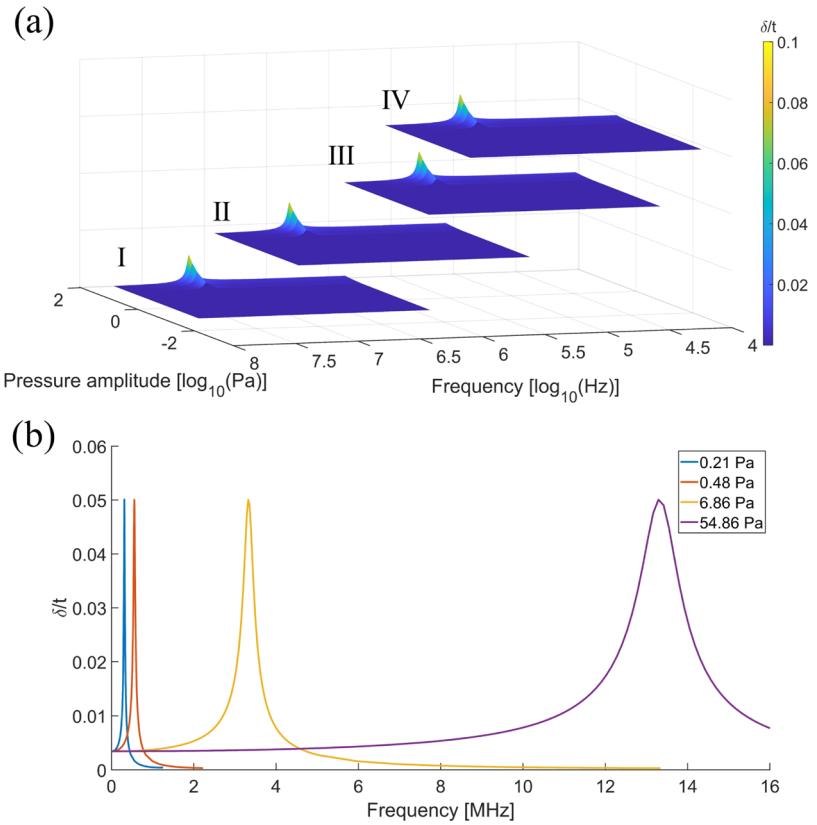

Figure 6. Results of dynamic pressure response analysis: (a) dependence of ribbon deflection on pressure amplitude and its frequency. The roman numbers denote the different ribbon structures, so I—1, II—2, III—5, and IV—7 μm. The color over the surface is proportional to δ/t. (b) Ribbon response curve (δ/t vs frequency); the pressure amplitude for each ribbon was selected to achieve the same amplitude at resonance.

act with force in the direction parallel to its layers. Most of the experiments[16,47−49] were carried out focusing only on examining such vertical forces. According to our simulations, the first three vibrational eigenmodes of the PNR have the following polarizations: mode 1 is horizontal, mode 2 is vertical, and mode 3 is horizontal. Therefore, mode 2 is the most amplified, as it is polarized in the direction parallel to vertical forces. The polarization of all of the described modes was investigated, and the results are presented in Figure 5c. The analysis shows that the modes are characterized by a pure linear polarization, i.e., the plane of their vibrations is fixed. Similar results regarding polarization were achieved by Rouhi and Ansari[50] and Li et al.[51] while they studied graphene nanoribbons.

In the case of normal mode calculations, the common approach is to approximate the oscillating structure as an elastic beam. The normal modes of the isotropic beam[52] with two ends fixed to terminals are given by eq 1

$$\omega = \alpha_i^2 \sqrt{\frac{EJ}{\mu}}, \ \alpha_i l = \frac{2i+1}{2}\pi \tag{1}$$

where l is the beam length, E is Young's modulus, J is the moment of inertia of the beam cross section, and μ is the linear density of the beam.

The dynamic simulations allowed us to investigate how the examined set of PNRs will behave under the influence of an oscillating excitation. PNRs with lengths of 1, 2, 5, and 7 μm were subjected to a sinusoidal oscillating pressure. In this analysis, the damping is an important factor along with the stiffness of the ribbon. The stiffness was calculated in this work by DFT. The damping factor of the nanostructures was assumed to be 3×10^{-2} based on a previous work.[53] The graph in Figure 6a shows how the maximum PNR deflection depends on the frequency and amplitude of the excitation. The obvious resonance peak stands out for each deflection surface; however, its position on the pressure/frequency plane varies. This information is important for the design of devices from PNRs since it allows for estimation of the maximal deflection of the ribbon, thus setting the requirements for the groove sizes. Moreover, it can also provide valid information about the magnitude of strain in the ribbon at a specific deflection, which is also important since many properties of phosphorene are bound with strain.

From the obtained data, similar to PNRs subjected to periodic excitation, the PNRs behave similarly to those subjected to static loading. PNR whippiness is inversely proportional to length. A similar effect was observed in graphene structures,[54] which suggests no significant mechanical behavior difference between PNR and graphene ribbons in regard to static loading tests. In Figure 6b, the image of resonance peaks is presented. Notably, the magnitude of pressure for each presented curve is not the same, so the amplitude of deflection in resonance is equal. The position of each peak indicates the mechanical resonance frequency. This frequency is equal to 0.313, 0.555, 3.325, and 13.29 MHz for nanoribbons with lengths of 7, 5, 2, and 1 μm, respectively. Considering the factor $\sqrt{1-2\zeta^2}$ caused by damping ζ, the resonance frequency equals the normal mode 2 frequency. This proves that both simulations are consistent.

https://doi.org/10.1021/acs.jpcc.2c04500
J. Phys. Chem. C 2022, 126, 14219−14228

In summary, there are multiple possible approaches for simulating the mechanical behavior of nanostructures: ab initio DFT approach,[55] force-field molecular dynamics,[56,57] FEM,[49] or analytical solution of continuum models.[58] Each of them has its own unique advantages, but the key factors are computational complexity and versatility in terms of nanomaterials. The generally good trade-off between the cost and versatility is presented by the force-field approach. However, even this method is mainly used for quasi-static deflection analysis[59] in regard to the simulation of nanoribbons with a high aspect ratio. In this work, the simulation of the dynamical behavior of the nanoribbons was the primary concern, so the hybrid DFT-FEM simulations were more favorable.

4. CONCLUSIONS

In conclusion, the obtained values of Young's modulus and Poisson's ratio refer to the nanoribbons and not to the 2D nanolayers. The results obtained for volumetric structures or even for 2D structures do not reflect the mechanical properties of 1D structures, so they should not be used for modeling phosphorene bridges by the FEM. For example, Young's modulus for single-layer phosphorene is equal to 194.5 GPa[60] and simulated in the described results for the single-layer nanoribbon of 134 GPa. The obtained values of Young's modulus and Poisson's coefficient differ significantly from those known from measurements for phosphorene nanolayers and phosphorene microstructures. This deviation can be attributed to the strong edge stress occurring in ultrathin nanoribbons. This stress disturbs the symmetry of the nanolayer,[24] so the 1 nm width PNR structure mechanically behaves more like a nanolayer with linear defects rather than pristine phosphorene. The presented ab initio simulations can provide useful data regarding the mechanical properties of the structures, regardless of whether experimental results are available for a particular kind of material.

The results achieved with the simulations confirm the previously known phenomenon; that is, a decrease in Young's modulus occurs with an increase in the number of layers and, in some cases, the occurrence of a negative Poisson's ratio. In the case of normal mode modeling, modeling using a rigidly fixed beam model produced similar results to FEM modeling. However, FEM allows for mode polarization study, which is not as simple using the analytical approach.

Considering different simulation methods of the mechanical behavior of nanostructures, such as the DFT ab initio, force-field MD, FEM, and analytical continuum model, a compromise between computational complexity and versatility should be established. As a solution to this issue, the hybrid approach was proposed in the article. FEM is applied for the continuum model of the structure to perform dynamical response analysis. The mechanical properties of the structure were calculated using the ab initio DFT approach. The authors suppose that wider application of this approach could accelerate the design of devices from phosphorene.

AUTHOR INFORMATION

Corresponding Author

Krzysztof Pyrchla − *Department of Metrology and Optoelectronics, Faculty of Electronics, Telecommunications and Informatics, Gdańsk University of Technology, 80-233 Gdańsk, Poland;* orcid.org/0000-0001-6027-7341; Phone: +48691041789; Email: krzysztof.pyrchla@pg.edu.pl

Author

Robert Bogdanowicz − *Department of Metrology and Optoelectronics, Faculty of Electronics, Telecommunications and Informatics, Gdańsk University of Technology, 80-233 Gdańsk, Poland;* orcid.org/0000-0002-7543-2620

Complete contact information is available at: https://pubs.acs.org/10.1021/acs.jpcc.2c04500

Notes

The authors declare no competing financial interest.

ACKNOWLEDGMENTS

This work was financed from the budget funds for science for the years 2019/2023 as a research project in the "Diamond Grant" program framework no. 0063/DIA/2019/48. The authors gratefully acknowledge financial support in part from the Polish National Science Centre (NCN) under grant no. 2016/22/E/ST7/00102.

REFERENCES

(1) Wang, F.; Ma, Z.; Wei, Y.; Huang, P.; Zhang, X. Switchable Electric Polarization of Phosphorene in Mixed Dimensional van Der Waals Heterostructure. *Appl. Surf. Sci.* **2021**, *563*, No. 150276.

(2) Watts, M. C.; Picco, L.; Russell-Pavier, F. S.; Cullen, P. L.; Miller, T. S.; Szymon, P.; Payton, O. D.; Skipper, N. T.; Tileli, V.; Howard, C. A.; et al. Production of Phosphorene Nanoribbons. *Nature* **2019**, *568*, 216−220.

(3) Liu, Z.; Sun, Y.; Cao, H.; Xie, D.; Li, W.; Wang, J.; Cheetham, A. K. Unzipping of Black Phosphorus to Form Zigzag-Phosphorene Nanobelts. *Nat. Commun.* **2020**, *11*, No. 3917.

(4) Yu, Y.; Yao, J.; Niu, X.; Xing, B.; Liu, Y.; Wu, X.; Li, M.; Yan, X.; Sha, J.; Wang, Y. Synthesis and Electrical Properties of Single Crystalline Black Phosphorus Nanoribbons. *CrystEngComm* **2020**, *22*, 3824−3830.

(5) Masih Das, P.; Danda, G.; Cupo, A.; Parkin, W. M.; Liang, L.; Kharche, N.; Ling, X.; Huang, S.; Dresselhaus, M. S.; Meunier, V.; Drndić, M. Controlled Sculpture of Black Phosphorus Nanoribbons. *ACS Nano* **2016**, *10*, 5687−5695.

(6) Yang, Y. R.; Zhang, Z. Q.; Gu, L.; Fu, H. H. Spin-Dependent Seebeck Effect in Zigzag Black Phosphorene Nanoribbons. *RSC Adv.* **2016**, *6*, 44019−44023.

(7) Tran, V.; Yang, L. Scaling Laws for the Band Gap and Optical Response of Phosphorene Nanoribbons. *Phys. Rev. B* **2014**, *89*, No. 245407.

(8) Lee, S.; Yang, F.; Suh, J.; Yang, S.; Lee, Y.; Li, G.; Choe, H. S.; Suslu, A.; Chen, Y.; Ko, C.; et al. Anisotropic In-Plane Thermal Conductivity of Black Phosphorus Nanoribbons at Temperatures Higher than 100 K. *Nat. Commun.* **2015**, *6*, No. 7261.

(9) Galluzzi, M.; Zhang, Y.; Yu, X.-F. Mechanical Properties and Applications of 2D Black Phosphorus. *J. Appl. Phys.* **2020**, *128*, No. 230903.

(10) Zhao, Y.; Zhang, G.; Nai, M. H.; Ding, G.; Li, D.; Liu, Y.; Hippalgaonkar, K.; Lim, C. T.; Chi, D.; Li, B.; et al. Probing the Physical Origin of Anisotropic Thermal Transport in Black Phosphorus Nanoribbons. *Adv. Mater.* **2018**, *30*, No. 1804928.

(11) Sun, J.; Li, X.; Ullrich, C. A.; Yang, J. Excitons in Bent Black Phosphorus Nanoribbons: Multiple Excitonic Funnels. *Mater. Today Adv.* **2020**, No. 100096.

(12) Yang, C. H.; Li, Q. F.; Chen, Y. Y.; Xu, W. Orientation and Strain Dependence of Optical Absorption in Black Phosphorene. *Phys. E* **2019**, *112*, 1−5.

(13) Akhtar, M.; Zhang, C.; Rajapakse, M.; Musa, M. R. K.; Yu, M.; Sumanasekera, G.; Jasinski, J. B. Bilayer Phosphorene under High Pressure:: In Situ Raman Spectroscopy. *Phys. Chem. Chem. Phys.* **2019**, *21*, 7298−7304.

(14) Pyrchla, K.; Bogdanowicz, R. Density Functional LCAO Calculations of Vibrational Modes and Phonon Density of States in

the Strained Single-Layer Phosphorene. *Appl. Surf. Sci.* **2020**, *528*, No. 147033.
(15) Zhang, W.; Yin, J.; Zhang, P.; Ding, Y. Strain/Stress Engineering on the Mechanical and Electronic Properties of Phosphorene Nanosheets and Nanotubes. *RSC Adv.* **2017**, *7*, 51466−51474.
(16) Chen, H.; Huang, P.; Guo, D.; Xie, G. Anisotropic Mechanical Properties of Black Phosphorus Nanoribbons. *J. Phys. Chem. C* **2016**, *120*, 29491−29497.
(17) Li, J.; Gao, Z.; Ke, X.; Lv, Y.; Zhang, H.; Chen, W.; Tian, W.; Sun, H.; Jiang, S.; Zhou, X.; Zuo, T.; et al. Growth of Black Phosphorus Nanobelts and Microbelts. *Small* **2018**, *14*, No. 1702501.
(18) Macewicz, L.; Pyrchla, K.; Bogdanowicz, R.; Sumanasekera, G.; Jasinski, J. B. Chemical Vapor Transport Route toward Black Phosphorus Nanobelts and Nanoribbons. *J. Phys. Chem. Lett.* **2021**, *12*, 8347−8354.
(19) Wei, Q.; Peng, X. Superior Mechanical Flexibility of Phosphorene and Few-Layer Black Phosphorus. *Appl. Phys. Lett.* **2014**, *104*, No. 251915.
(20) Jing, Y.; Zhang, X.; Zhou, Z. Phosphorene: What Can We Know from Computations? *Wiley Interdiscip. Rev.: Comput. Mol. Sci.* **2016**, *6*, 5−19.
(21) Kou, L.; Chen, C.; Smith, S. C. Phosphorene: Fabrication, Properties, and Applications. *J. Phys. Chem. Lett.* **2015**, *6*, 2794−2805.
(22) Miao, Y.; He, L. Mechanical and Electronic Properties of 2D Black Phosphorene Nanoribbons: A First-Principles Study. *IOP Conf. Ser. Earth Environ. Sci.* **2021**, *702*, No. 012022.
(23) Bets, K. V.; Yakobson, B. I. Spontaneous Twist and Intrinsic Instabilities of Pristine Graphene Nanoribbons. *Nano Res.* **2009**, *2*, 161−166.
(24) Sorkin, V.; Cai, Y.; Ong, Z.; Zhang, G.; Zhang, Y. W. Recent Advances in the Study of Phosphorene and Its Nanostructures. *Crit. Rev. Solid State Mater. Sci.* **2017**, *42*, 1−82.
(25) Wang, C. M.; Tan, V. B. C.; Zhang, Y. Y. Timoshenko Beam Model for Vibration Analysis of Multi-Walled Carbon Nanotubes. *J. Sound Vib.* **2006**, *294*, 1060−1072.
(26) Liew, K. M.; Wang, Q. Analysis of Wave Propagation in Carbon Nanotubes via Elastic Shell Theories. *Int. J. Eng. Sci.* **2007**, *45*, 227−241.
(27) Li, C.; Chou, T. W. A Structural Mechanics Approach for the Analysis of Carbon Nanotubes. *Int. J. Solids Struct.* **2003**, *40*, 2487−2499.
(28) Zhang, Y.; Liu, G.; Han, X. Transverse Vibrations of Double-Walled Carbon Nanotubes under Compressive Axial Load. *Phys. Lett. A* **2005**, *340*, 258−266.
(29) Chang, W. J.; Lee, H. L. Free Vibration of a Single-Walled Carbon Nanotube Containing a Fluid Flow Using the Timoshenko Beam Model. *Phys. Lett. A* **2009**, *373*, 982−985.
(30) Tserpes, K. I.; Papanikos, P. Finite Element Modeling of Single-Walled Carbon Nanotubes. *Composites, Part B* **2005**, *36*, 468−477.
(31) Arash, B.; Ansari, R. Evaluation of Nonlocal Parameter in the Vibrations of Single-Walled Carbon Nanotubes with Initial Strain. *Phys. E* **2010**, *42*, 2058−2064.
(32) Ansari, R.; Rouhi, S. Atomistic Finite Element Model for Axial Buckling of Single-Walled Carbon Nanotubes. *Phys. E* **2010**, *43*, 58−69.
(33) Huang, L. Y.; Zhang, X.; Zhang, M.; Lu, G. Optically Inactive Defects in Monolayer and Bilayer Phosphorene: A First-Principles Study. *Phys. Rev. Mater.* **2018**, *2*, 1−8.
(34) Wang, J. Y.; Li, Y.; Zhan, Z. Y.; Li, T.; Zhen, L.; Xu, C. Y. Elastic Properties of Suspended Black Phosphorus Nanosheets. *Appl. Phys. Lett.* **2016**, *108*, No. 4727.
(35) Jiang, J. W.; Park, H. S. Negative Poisson's Ratio in Single-Layer Black Phosphorus. *Nat. Commun.* **2014**, *5*, No. 4727.
(36) Du, Y.; Maassen, J.; Wu, W.; Luo, Z.; Xu, X.; Ye, P. D. Auxetic Black Phosphorus: A 2D Material with Negative Poisson's Ratio. *Nano Lett.* **2016**, *16*, 6701−6708.
(37) Jiang, J. W.; Rabczuk, T.; Park, H. S. A Stillinger-Weber Potential for Single-Layered Black Phosphorus, and the Importance of Cross-Pucker Interactions for a Negative Poisson's Ratio and Edge Stress-Induced Bending. *Nanoscale* **2015**, *7*, 6059−6068.
(38) Carmel, S.; Subramanian, S.; Rathinam, R.; Bhattacharyya, A. Twisted Monolayer Black Phosphorus Nanoribbbons: Tunable Electronic and Optical Properties. *J. Appl. Phys.* **2020**, *127*, No. 094303.
(39) Kang, P.; Zhang, W.; Michaud-Rioux, V.; Wang, X.; Yun, J.; Guo, H. Twistronics in Tensile Strained Bilayer Black Phosphorus. *Nanoscale* **2020**, *12*, 12909−12916.
(40) Zhang, R. Y.; Zheng, J. M.; Jiang, Z. Y. Strain Effects on Properties of Phosphorene and Phosphorene Nanoribbons: A DFT and Tight Binding Study. *Chin. Phys. Lett.* **2017**, *35*, No. 017302.
(41) Wei, N.; Xu, L.; Wang, H. Q.; Zheng, J. C. Strain Engineering of Thermal Conductivity in Graphene Sheets and Nanoribbons: A Demonstration of Magic Flexibility. *Nanotechnology* **2011**, *22*, No. 105705.
(42) Namnabat, M. S.; Barzegar, A.; Javanbakht, M. Finite Element Buckling Analysis of Double-Layered Graphene Nanoribbons. *Mater. Res. Express* **2019**, *6*, No. 055023.
(43) Song, L.; Guo, Z.; Chai, G. B.; Wang, Z.; Li, Y.; Luan, Y. A Finite Element Method to Investigate the Elastic Properties of Pillared Graphene Sheet under Different Conditions. *Carbon* **2018**, *140*, 210−217.
(44) Aghdasi, P.; Ansari, R.; Rouhi, S.; Yousefi, S. A DFT-Based Finite Element Approach for Studying Elastic Properties, Buckling and Vibration of the Arsenene. *J. Mol. Graphics Modell.* **2020**, *101*, No. 107725.
(45) Rostami chayjan, M.; Ahmadi, I.; Khoeini, F. Highly Tunable Charge Transport in Defective Graphene Nanoribbons under External Local Forces and Constraints: A Hybrid Computational Study. *Results Phys.* **2021**, *20*, No. 103770.
(46) Pica, M. Chemistry of Phosphorene: Synthesis, Functionalization and Biomedical Applications in an Update Review. 2020.
(47) Shimada, T.; Huang, K.; Van Lich, L.; Ozaki, N.; Jang, B.; Kitamura, T. Beyond Conventional Nonlinear Fracture Mechanics in Graphene Nanoribbons. *Nanoscale* **2020**, *12*, 18363−18370.
(48) Liu, D.; Daniels, C.; Meunier, V.; Every, A. G.; Tománek, D. In-Plane Breathing and Shear Modes in Low-Dimensional Nanostructures. *Carbon* **2020**, *157*, 364−370.
(49) Pang, H.; Huang, P.; Zhuo, W.; Li, M.; Gao, C.; Guo, D. Hysteresis and Its Impact on Characterization of Mechanical Properties of Suspended Monolayer Molybdenum-Disulfide Sheets. *Phys. Chem. Chem. Phys.* **2019**, *21*, 7454−7461.
(50) Rouhi, S.; Ansari, R. Atomistic Finite Element Model for Axial Buckling and Vibration Analysis of Single-Layered Graphene Sheets. *Phys. E* **2012**, *44*, 764−772.
(51) Li, Y.; Yu, C.; Gan, Y.; Jiang, P.; Yu, J.; Ou, Y.; Zou, D. F.; Huang, C.; Wang, J.; Jia, T.; et al. Mapping the Elastic Properties of Two-Dimensional MoS2 via Bimodal Atomic Force Microscopy and Finite Element Simulation. *npj Comput. Mater.* **2018**, *4*, No. 49.
(52) Rao, S. S. Vibration of Continuous Systems. 2007 DOI: 10.1002/9780470117866.
(53) Li, B.; Wei, Y.; Meng, F.; Ou, P.; Chen, Y.; Che, L.; Chen, C.; Song, J. Atomistic Simulations of Vibration and Damping in Three-Dimensional Graphene Honeycomb Nanomechanical Resonators. *Superlattices Microstruct.* **2020**, *139*, No. 106420.
(54) Neek-Amal, M.; Peeters, F. M. Graphene Nanoribbons Subjected to Axial Stress. *Phys. Rev. B* **2010**, *82*, No. 085432.
(55) Mortazavi, B.; Silani, M.; Podryabinkin, E. V.; Rabczuk, T.; Zhuang, X.; Shapeev, A. V. First-Principles Multiscale Modeling of Mechanical Properties in Graphene/Borophene Heterostructures Empowered by Machine-Learning Interatomic Potentials. *Adv. Mater.* **2021**, *33*, No. 2102807.
(56) Jiang, J.-W. Parametrization of Stillinger−Weber Potential Based on Valence Force Field Model: Application to Single-Layer MoS_2 and Black Phosphorus. *Nanotechnology* **2015**, *26*, No. 315706.
(57) Xiao, H.; Shi, X.; Hao, F.; Liao, X.; Zhang, Y.; Chen, X. Development of a Transferable Reactive Force Field of P/H Systems:

Application to the Chemical and Mechanical Properties of Phosphorene. *J. Phys. Chem. A* **2017**, *121*, 6135−6149.
(58) Bakhtiari, I.; Behrouz, S. J.; Rahmani, O. Nonlinear Forced Vibration of a Curved Micro Beam with a Surface-Mounted Light-Driven Actuator. *Commun. Nonlinear Sci. Numer. Simul.* **2020**, *91*, No. 105420.
(59) Kang, J. W.; Lee, S. Molecular Dynamics Study on the Bending Rigidity of Graphene Nanoribbons. *Comput. Mater. Sci.* **2013**, *74*, 107−113.
(60) Eslamibidgoli, M. J.; Eikerling, M. H. Mechanical and Chemical Stability of Monolayer Black Phosphorous Studied by Density Functional Theory Simulations. *J. Phys. Chem. C* **2018**, *122*, 22366−22373.

https://doi.org/10.1021/acs.jpcc.2c04500
J. Phys. Chem. C 2022, 126, 14219−14228